A two-dimensional Fourier transform method for the measurement of propagating multimode signals

D. Alleyne and P. Cawley
Department of Mechanical Engineering, Imperial College, London SW7 2BX, England

(Received 25 May 1990; accepted for publication 25 September 1990)

A technique for the analysis of propagating multimode signals is presented. The method involves a two-dimensional Fourier transformation of the time history of the waves received at a series of equally spaced positions along the propagation path. The technique has been used to measure the amplitudes and velocities of the Lamb waves propagating in a plate, the output of the transform being presented using an isometric projection which gives a three-dimensional view of the wave-number dispersion curves. The results of numerical and experimental studies to measure the dispersion curves of Lamb waves propagating in 0.5-, 2.0-, and 3.0-mm-thick steel plates are presented. The results are in good agreement with analytical predictions and show the effectiveness of using the two-dimensional Fourier transform (2-D FFT) method to identify and measure the amplitudes of individual Lamb modes.

PACS numbers: 43.35.Mr, 43.35.Zc, 43.40.Dx

INTRODUCTION

Conventional time domain methods of measuring the amplitudes and velocities of stress waves generally require minimal signal processing and are often the easiest to apply. If the time history of a wave packet consisting of a single mode can be resolved separately from other wave packets in the time domain then its amplitude may be measured, and its group velocity may be determined by measuring the time it takes to propagate between two positions a known distance apart. However, if the time record is composed of a number of superimposed wave packets, it may not be possible to measure amplitudes or group velocity.

Early investigations to detect different echoes in seismic signals deconvolved the time record using a cepstrum analysis, which is a logarithmic conversion of the spectrum of the time record (see, for example, Randall, 1987). More recently, spectral methods have been used by Sachse and Pao (1978) and Pialucha *et al.* (1989) to measure phase and group velocity by transforming the time domain data to the frequency domain, where data interpretation may be easier.

Since Worlton (1957) used Lamb waves to nondestructively test plates there has been a great deal of interest in the application of plate waves in NDT. Many workers (see, for example, Rokhlin and Bendec, 1983) have shown that Lamb waves may be used in localized, detailed NDT applications, where the detectability of a given defect may be optimized by choosing the most suitable modes at the appropriate frequency–thickness product. As they are essentially two-dimensional, Lamb waves are attenuated less rapidly than three-dimensional bulk waves, and hence may be propagated over considerable distances. Therefore, Lamb waves have been used by many workers in long-range NDT applications, where a coarse and quick inspection of large platelike structures may be carried out (see, for example, Ball and Shewring, 1976). However, more than one propagating Lamb wave always exists and velocity dispersion is usually evident. The time history of the response of the plate to an imposed excitation can therefore only be used to measure Lamb wave amplitudes and velocities approximately, because the shape of the response signal will be different at different positions along the surface of the plate. Also, if the group velocities of the Lamb waves excited are similar, a considerable propagation distance is required before they can be resolved in the time domain.

Mal *et al.* (1988), Chimenti and Nayfeh (1985), and others have used a reflection coefficient technique to measure the dispersion curves of leaky Lamb waves to determine material properties. However, the relative amplitudes of the Lamb waves present (mode purity) cannot easily be determined. Rose *et al.* (1983) have developed a method using a similarity coefficient, where the spectrum of received signals is compared with a reference or good spectrum. This is primarily a statistical correlation technique used in the NDT of tubular structures. Others have used time domain correlation methods (Avioli, 1988), where the received signal is processed to obtain a signal envelope that may be gated to measure the dispersion curves. Also, Zhang *et al.* (1985) have used a photoelastic visualization technique to investigate Lamb wave excitation and propagation qualitatively.

The two-dimensional Fourier transform (2-D FFT) technique presented here is an alternative method of measuring the dispersion curves of Lamb waves quantitatively. It overcomes the problems of multiple modes and dispersion by transforming the received amplitude–time record to amplitude–wave-number records at discrete frequencies, where individual Lamb waves may be resolved and their amplitudes measured. The major advantage of the 2-D FFT method, which is of great importance in NDT applications, is that Lamb wave amplitudes *and* velocities are measured. Propagation distances may be large and are limited only by the signal-to-noise ratio.

The first part of the paper presents basic theory relating to the computation of Lamb wave dispersion curves and

 0001-4966/91/031159-10$00.80

mode shapes. The numerical and experimental results of Lamb wave propagation and reflection in steel plates are then presented and compared.

I. LAMB WAVE BACKGROUND

A. Dispersion curves and deflected shapes

In the analysis that follows, the material is assumed to be linear elastic, isotropic, homogeneous, nonpiezoelectric, and nonabsorbing. Assuming a harmonic wave propagating in a plate with the coordinate system shown in Fig. 1, the displacement on the surface, $\mathbf{u}(x,t)$, may be described by a general analytic expression given by Brekhovskikh (1960) as,

$$\mathbf{u}(x,t) = \mathbf{A}(\omega)e^{i(\omega t - kx - \theta)}, \tag{1}$$

where $\mathbf{A}(\omega)$ is a frequency-dependent amplitude constant, $\omega = 2\pi f$ is the angular frequency, the wave number $k = \omega/c$, c is the phase velocity, and θ denotes the phase.

Lamb waves are two-dimensional propagating vibrations in free plates, with displacements that may be symmetric (symmetric modes) or antisymmetric (antisymmetric modes) with respect to the middle of the plate, and are eigensolutions of characteristic equations, hence the term free or normal modes. The velocities of all Lamb waves are dispersive and in any plate of thickness, $2d$, at a particular frequency, f, there will be a finite number of propagating modes, which may be determined from the number of real roots of the Rayleigh–Lamb equation. The phase velocities or wave numbers of Lamb waves as a function of the frequency–thickness product may be obtained by solving the following transcendental equations:

$$\frac{\tan \omega d\sqrt{(c^2 - c_2^2)/c_2^2c^2}}{\tan \omega d\sqrt{(c^2 - c_1^2)/c_1^2c^2}} + \left(4\frac{\sqrt{[(c/c_1)^2 - 1][(c/c_2)^2 - 1]}}{[2 - (c/c_2)^2]^2}\right)^{\pm 1} = 0. \tag{2}$$

The $+ve$ and $-ve$ signs relate to symmetric and antisymmetric Lamb waves, respectively, and c_1 and c_2 are the bulk longitudinal and shear wave velocities, respectively. The positive and negative real roots of Eq. (2) correspond to propagating harmonic waves in the $+ve$ and $-ve$ x directions, respectively, while the imaginary or complex roots relate to nonpropagating spatially varying vibrations, which are of importance in forced and transient wave motion. The group velocity, $c_g = \partial\omega/\partial k$, may be calculated once the phase velocity or wave number as a function of the frequency–thickness product is known. Figure 2 shows the predicted Lamb wave-number dispersion curves for the first five symmetric and antisymmetric Lamb waves of a steel plate, where $c_1 = 5960$ m/s and $c_2 = 3260$ m/s. The through thickness displacement components of symmetric Lamb waves are obtained from the following equations:

$$u_s = Ak_s i\left(\frac{\cosh q_s z}{\sinh q_s d} - \frac{2q_s s_s}{k_s^2 - s_s^2}\frac{\cosh s_s z}{\sinh s_s d}\right)e^{i(k_s x - \omega t)} \tag{3}$$

and

$$w_s = Aq_s\left(\frac{\sinh q_s z}{\sinh q_s d} - \frac{2k_s^2}{k_s^2 + s_s^2}\frac{\sinh s_s z}{\sinh s_s d}\right)e^{i(k_s x - \omega t)}, \tag{4}$$

where u_s and w_s are the displacements in the x and z directions, respectively, k_s is the wave number of the symmetric Lamb modes, $q_s^2 = k_s^2 - k_2^2$, and $s_s^2 = k_s^2 - k_1^2$. Similar relations for the antisymmetric modes may be obtained by changing the subscript s to a and replacing sinh by cosh and vice versa. Figure 3(a) and (b) show the deflected mode shapes of a_0 and a_1, respectively, at 3 MHz mm.

II. SPECTRAL METHODS

A. A two-dimensional spectral method

The key problem associated with the quantitative measurement of the characteristics of propagating Lamb waves is that more than one mode can exist at any given frequency. The 2-D FFT method described in this section is an extension of the one-dimensional phase spectrum method developed by Sachse and Pao (1978) for the measurement of the velocity of stress waves. Broadband excitation signals from transducers of finite dimensions generally excite more than one propagating mode. Therefore, the phase spectrum method of measuring the dispersion curves is not easy to apply in frequency–thickness regions above 1.63 MHz mm (the cutoff value of the a_1 mode in steel), since it implicitly assumes that only a single mode is present.

Propagating Lamb waves are sinusoidal in both the frequency and spatial domains, as can be seen from Eq. (1). Therefore, a temporal Fourier transform may be carried out to go from the time to frequency domain, then a spatial Four-

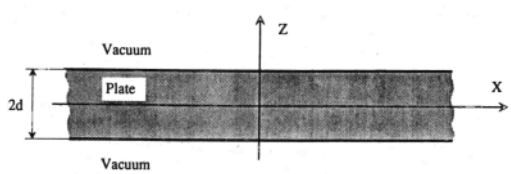

FIG. 1. Schematic representation of the plate geometry and coordinate system used.

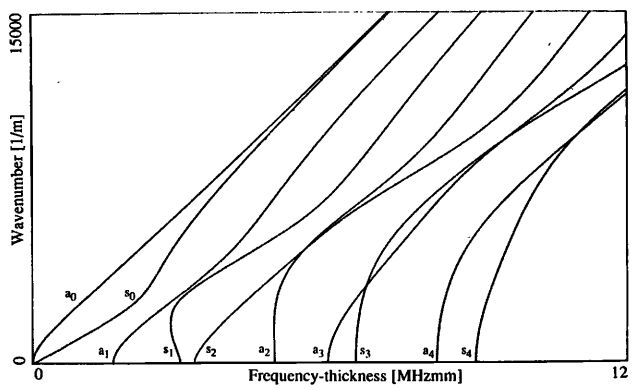

FIG. 2. Lamb wave wave-number dispersion curves for steel, where $c_1 = 5960$ m/s and $c_2 = 3260$ m/s.

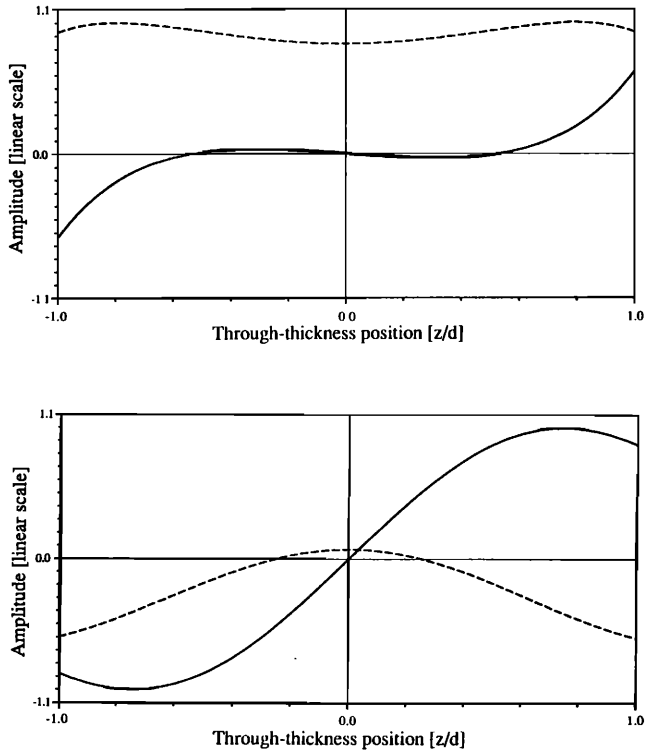

FIG. 3. (a) The through-thickness deflected mode shape of a_0 at 3 MHz mm, where c_1 and c_2 are the same as in Fig. 2:———x-direction displacement; ----z-direction displacements. (b) The through-thickness deflected mode shape of a_1 at 3 MHz mm, where c_1 and c_2 are the same as in Fig. 2:——x-direction displacement; ---- z-direction displacements.

ier transform may be carried out to go to the frequency–wave-number domain, where the amplitudes and wave numbers of individual modes may be measured.

Applying spatial Fourier methods in practice to data gained experimentally or numerically requires us to carry out a two-dimensional Fourier transform of Eq. (1) giving

$$H(k,f) = \int_{-\infty}^{+\infty} \int_{-\infty}^{+\infty} \mathbf{u}(x,t) e^{-i(kx+\omega t)}\, dx\, dt. \qquad (5)$$

The discrete two-dimensional Fourier transform may be defined in a similar way to the one-dimensional DFT given in, for example, Newland (1984). The result of this transformation will be a two-dimensional array of amplitudes at discrete frequencies and wavenumbers. As in the one-dimensional case, aliasing must be avoided by sampling the data at a sufficiently high frequency in time and wave number in space. Usually the signal will not be periodic within the temporal and spatial sampling windows and leakage will occur. Window functions such as the Hanning window may be used to reduce this leakage, and zeros may be padded to the end of the signal to enable the frequency and wave number of the maximum amplitude to be determined more accurately. Details of the fast Fourier transform algorithm, aliasing, leakage, zero padding, and other effects associated with discrete Fourier transforms may be found in standard texts, for example, Randall (1987).

The two-dimensional Fourier transform method is applied by carrying out a Fourier transform of the time history of the response at each position monitored to obtain a frequency spectrum for each position. At this stage, an array with the spectral information for each position in its respective column is obtained. A spatial Fourier transform of the vector (row) formed by the components at a given frequency then gives the amplitude–wave-number–frequency information. In practice a two-dimensional fast Fourier transform algorithm (2-D FFT) may be used. In contrast to the method developed by Sachse and Pao (1978) this method enables the amplitude and velocity of different modes propagating at the same frequency to be determined.

III. NUMERICAL MODELING

A. Background

Explicit finite difference schemes were the first numerical methods to be applied to investigate the propagation and scattering of stress waves. Temple (1988) has used finite difference schemes to model bulk wave propagation in inhomogeneous media and Bond *et al.* (1984) have used finite difference schemes to model the scattering of stress waves from surface features. Blake (1988) used both finite difference and finite element schemes to investigate stress wave propagation and scattering. However, when using finite difference schemes that incorporated sophisticated routines to cater for free boundaries, he was unable to obtain a stable solution for the reflection of Rayleigh waves along sloping free boundaries. He also showed that the surface node displacement errors of finite element schemes are smaller in comparison to those of finite difference schemes using the "body node" formulation. Free boundaries are readily accommodated by finite element schemes and they have the added advantages of flexibility, although they are computationally more expensive. In Lamb wave studies, a large percentage of the nodes are at free boundaries and the stresses of some modes are localized near the boundary. Therefore, the numerical modeling reported here was carried out using a finite element code, in which a central difference approximation was used to obtain the time marching solution.

The modeling of Lamb waves is problematic because they are dispersive, more than one mode is always possible and their through thickness deflected shape is a function of the frequency–thickness product. The velocity of the longitudinal wave (c_1), which is the fastest wave that can propagate in the plate, controls the computational time step that must be chosen so that a disturbance cannot propagate through a grid spacing in under one time step, while the lowest phase velocity, and hence the shortest wavelength, sets the maximum permissible grid spacing that must be chosen so that spatial aliasing due to the finite element discretization does not occur. All the work reported here was carried out using 8 noded quadrilateral elements and a uniform square mesh with more than 10 nodes per wavelength, which proved to be adequate.

An individual Lamb wave was launched from one end of the plate by applying a 5-cycle, 1-MHz sinusoidal tone burst, modulated temporally by a Hanning window function to limit the bandwidth. The amplitude of the x and z displacements at each node on the plate edge were given by the through thickness deflected shape calculated from Eqs. (3)

and (4). The form of the input function is shown in Fig. 4(a).

In the next section the results of finite element modeling investigations on 0.5-, 2.0-, and 3.0-mm steel plates will be presented. These results are used to show how the 2-D FFT method may be used to quantitatively analyze Lamb wave response signals before and after reflection from the free edge of the plate.

B. Finite element results without reflection

Finel, a finite element package developed at Imperial College (Hitchings, 1987), was used to model the plates; c_1 and c_2 were the same values used to calculate the dispersion curves of Fig. 2 and the density, $\rho = 8000$ kg/m^3. The time history of the response in the z direction on the plate surface at 64 equally spaced points in the x direction was recorded. In all the studies the sampling frequency was 10 MHz.

The finite element model of the 0.5-mm-thick plate was 200 mm long and the spatial sampling interval was 1 mm. Figure 4(a) and (b) show the normalized time histories of the response of the top surface of the plate at $x = 0$ and 100 mm, respectively, where the input at $x = 0$ was appropriate to excite only s_0. The response of the plate at $x = 100$ mm shows that the propagating wave is essentially nondispersive and the group velocity is 5.43 km/s. Figure 4(c) shows the result of carrying out a two-dimensional Fourier transform on the 64 monitored time histories between $x = 100$ mm and $x = 163$ mm. The results are presented in the form of a three-dimensional plot of amplitude versus frequency and wave number. The amplitude scale is linear and the units are arbitrary. (This scale is not shown to improve the clarity of the plot.) At each frequency, the amplitude is only significant at a single wave number, indicating that only one mode, in this case, s_0, is present. The amplitude reaches a maximum at a frequency of 1 MHz which is the center frequency of the excitation tone burst. A comparison of the 2-D FFT results and the theoretically predicted wave-number dispersion curve for s_0 is shown in Fig. 5. The numerical results are represented by squares and are the wave-number–frequency points at which the amplitudes in Fig. 4(c) are a maximum. The agreement is seen to be very good, the maximum error in wavenumber being less than 0.5%.

The finite element model of the 3-mm-thick plate was 125 mm long and the spatial sampling interval was 0.6 mm. The input at $x = 0$ was appropriate to excite only a_0 and Fig. 3(a) shows the amplitudes of the applied displacements used to launch a_0. The normalized time history of the response at $x = 50$ mm is shown in Fig. 6(a). The shape of the response of Fig. 6(a) is very similar to the excitation signal shown in Fig. 4(a). This indicates that a_0 is almost nondispersive at this frequency–thickness value and the maximum group velocity measured from the leading edge of the signal was 3.27 km/s. Figure 6(b) shows the normalized three-dimensional view of the amplitude–wave-number–frequen-

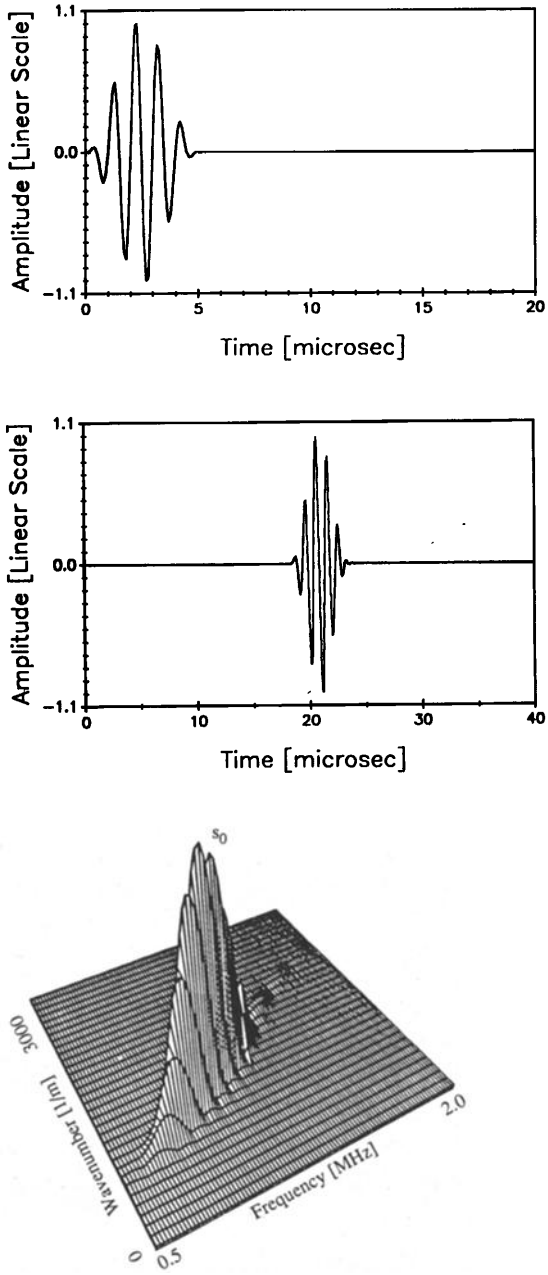

FIG. 4. (a) Normalized time history of the z displacement at $x = 0$ used in all the numerical tests. (b) Predicted normalized time history of the z displacement at $x = 100$ mm in a 0.5-mm plate when the input at $x = 0$ was designed to excite only s_0. (c) Normalized 3-D plot of the 2-D FFT results of the case given in (b), showing a single propagating mode, s_0.

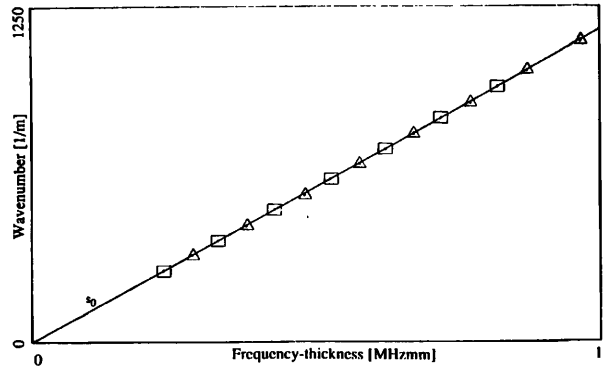

FIG. 5. A comparison of the finite element predictions and experimental results with the analytically generated dispersion curves for s_0. ——analytical predictions; ⊡ finite element predictions; △ experimental results.

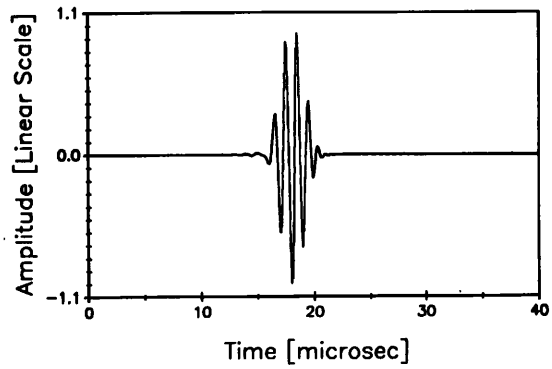

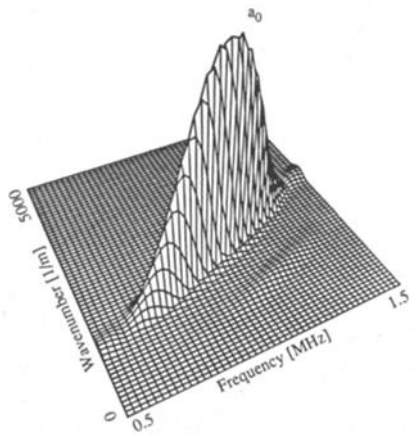

FIG. 6. (a) Predicted normalized time history at $x = 50$ mm in a 3-mm plate when the input at $x = 0$ was designed to excite only a_0. (b) Normalized 3-D plot of the 2-D FFT results of the case given in (a), showing a single propagating mode, a_0.

cy information, which was obtained by carrying out a two-dimensional Fourier transformation of the time histories of 64 equally spaced points from $x = 30$ mm to $x = 67.8$ mm. The maximum amplitude of the response of the plate is at 1 MHz, which is the center frequency of the excitation tone burst. At each discrete frequency in Fig. 6(b) the amplitude reaches a maximum at the wave-number corresponding to a_0. Since no other modes are evident in Fig. 6(b), it shows that in numerical studies, pure Lamb waves may be launched successfully in frequency–thickness regions where many modes with complicated mode shapes exist. This is of great importance in NDT, where for example, the sensitivity of individual Lamb waves to different defects may be studied separately. Figure 7 shows a comparison of the 2-D FFT results and the theoretically predicted wave-number dispersion curve. The numerical results were obtained as described above and the points relating to a_0 obtained from Fig. 6(b) are represented by circles. The agreement with the theoretical curve is excellent, the maximum error in wave number being less than 0.5%.

The finite element model of the 3-mm-thick plate when a_1 was launched at $x = 0$ was 125 mm long and the spatial sampling interval was 0.6 mm. Figure 3(b) shows the amplitudes of the applied displacements used to launch a_1 at $x = 0$. The normalized time history of the response at $x = 50$ mm is shown in Fig. 8(a), from which the maximum group

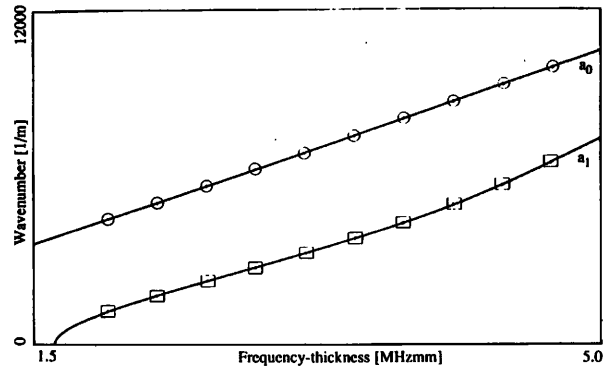

FIG. 7. A comparison of the finite element predictions with the analytically generated dispersion curves for a_0 and a_1: ——analytical predictions; ⊙ finite element predictions for a_0; ⊡ finite element predictions for a_1.

velocity measured from the leading edge of the signal is 3.84 km/s. The time history of the response of the plate to the excitation at $x = 0$ changes shape as the wave packet propagates from $x = 0$ to $x = 50$ mm [see Fig 4(a)], indicating that if the only propagating mode is a_1, then it is dispersive. Figure 8(b) shows the results of carrying out a two-dimensionally Fourier transform on the time histories of 64 equally spaced points between $x = 30$ mm and $x = 67.8$ mm. Again, the maximum amplitude of the response of the plate is at 1

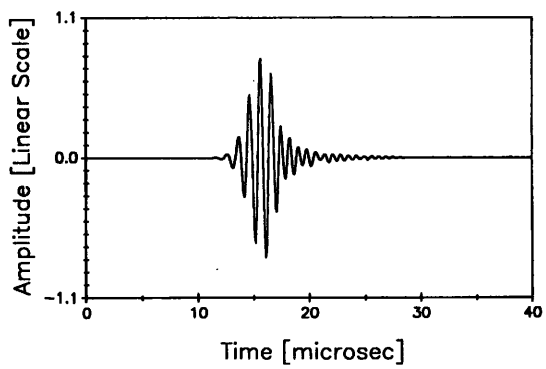

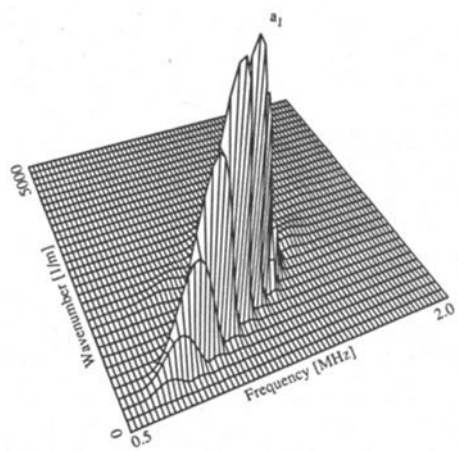

FIG. 8. (a) Predicted normalized time history at $x = 50$ mm in a 3-mm plate when the input at $x = 0$ was designed to excite only a_1. (b) Normalized 3-D plot of the 2-D FFT results of the case given in (a), showing a single propagating mode, a_1.

MHz, the centre frequency of the excitation tone burst. At each discrete frequency in Fig. 8(b), the maximum amplitude is seen at the wave number corresponding to a_1, and no other maximum is seen, indicating that a_1 is the only propagating mode. Figure 7 shows the comparison between the 2-D FFT results and the theoretically predicted wave-number dispersion curve, where the numerical results are obtained as described above and the points relating to a_1 are represented by squares. The agreement with the theoretical curve is excellent, the maximum error in wave number being less than 0.5%.

C. Finite element results with reflection

The finite element models used in the investigation of Lamb wave reflection from the free end of the plate were 3 mm thick and the material properties were the same as in the previous finite element studies.

Figure 9(a) shows the normalized time history of the response of a 125-mm-long finite element model at $x = 50$ mm, when the input at $x = 0$ was appropriate to excite only a_0. The duration of the test was long enough to include the response of the plate after reflection from the end of the plate. When $t \leqslant 40\ \mu s$ the response is identical to that of Fig. 6(a), a_0 is essentially nondispersive and the maximum group velocity is 3.266 km/s. On reflection from the end of the plate ($t \geqslant 40\ \mu s$) more than one propagating mode is present (a_0 is mode converted), but the modes are superimposed and their amplitudes cannot be determined from the time history of the response of the plate. Figure 9(b) shows the result of carrying out a two-dimensional Fourier transform on the time histories of the 64 equally spaced positions from $x = 30$ mm to $x = 67.8$ mm, when the incident signal ($t \leqslant 40\ \mu s$) was gated out. The maximum amplitude of the response of the plate is at 1 MHz, which is the center frequency of the excitation tone burst. However, at each discrete frequency in Fig. 9(b) there are two distinct wave numbers at which the amplitude is a maximum. These correspond to a_0 and a_1. Hence, there are two propagating modes and the amplitudes of the two modes are a function of frequency.

The amplitudes of a_0 and a_1, seen in Fig. 9(b) depend not only on the reflection coefficients of the waves at the end of the plate, but also on the frequency content of the excitation tone burst and on the amplitude of the z component of the deflected shape compared with the x component (only the z component is monitored). In order to be able to compare these results with analytically calculated reflection coefficients, it is necessary to normalize the amplitudes by dividing by the theoretically calculated z component at the surface. The reflection coefficients are then obtained in the normal way by dividing the response by the input. Figure 10 shows the reflection coefficients calculated in this manner from the data of Fig. 9(b). The agreement between the numerical results and theoretical predictions obtained using the theoretical approach described by Torvik (1967) are excellent, the maximum difference being less than 2%.

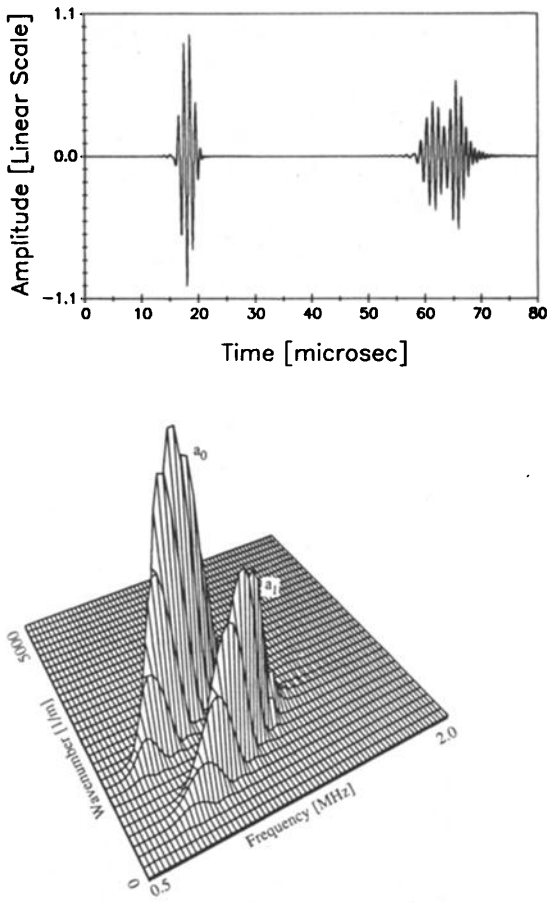

FIG. 9. (a) Predicted normalized time history at $x = 50$ mm in a 3-mm plate, showing the first passage of the a_0 wave and the reflection containing both a_0 and a_1 from the free end of the plate. (b) Normalized 3-D plot of the 2-D FFT results from the reflected wave shown in (a).

IV. EXPERIMENTAL INVESTIGATION

A. Procedure

The aim of the experimental investigation was to excite a single Lamb wave and to study its propagation. The instrumentation used is shown schematically in Fig. 11. A pulse from the pulse generator was used to simultaneously trigger the oscilloscope and the function generator that delivered a 5-cycle tone burst to the power amplifier. The power amplifier delivered the input signal to the transmitting transducer

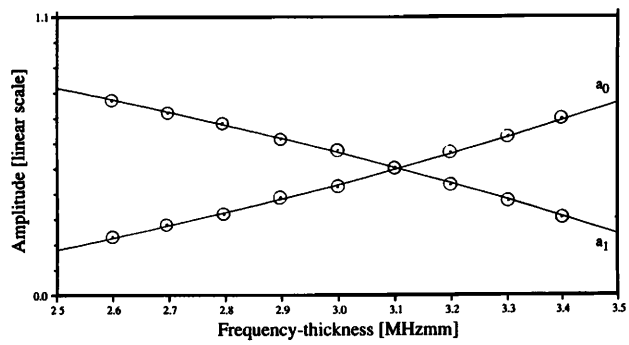

FIG. 10. The distribution of energy between a_0 adn a_1 after reflection from the free end of the plate when only a_0 was incident.—theoretical predictions using the method of Torvik (1967); ⊙ numerical results.

with a gain of 50 dB. The ultrasonic waves excited by the transmitting transducer propagated along the plate and were received by the receiving tranducer, the received signal being amplified and transferred to the oscilloscope for digital capture and display. The signals from the oscilloscope were transferred to the computer via the GPIB bus to be edited and then transferred to the spectrum analyzer, which was used to carry out the digital Fourier transformation. The resulting transformed data was transferred back to the computer for redisplaying and editing. Two variable-angle, constant emission point, 1-MHz broadband transducers were used in the experiments. A dial gauge measured the movement of the receiving transducer to obtain a constant spatial sampling interval and the above procedure was carried out at 64 successive positions along the surface of the plate to obtain the spatial records.

The accuracy of positioning the transducer in these experiments was about 2% of the spatial sampling interval. However, the quality of the coupling between the transducer and the plate probably varied as the transducer was indexed, which introduced errors. It should also be remembered that the measured response is integrated over the area of the transducer element. These problems could be reduced by using a transducer consisting of an array of small elements to capture the time histories.

The plates used in the experimental investigations were approximately 300 mm wide and 1 m long, and the average propagation distance was restricted to 200 mm in order to keep the signal-to-noise ratio high. Individual Lamb waves were selectively excited by applying the coincidence principle [see, for example, Worlton (1957), Jitsumori (1986), and many others]. The angle of incidence, θ, required for the excitation of the desired mode is calculated from $\theta = \sin^{-1}(c_L/c)$, where c_L is the phase velocity of a compression wave incident on the surface of the plate and c is the phase velocity of the Lamb wave to be excited. The variable angle transducers used in the experiments were 10 mm in diameter and were mounted in a perspex body, in which the compression wave velocity is 2.55 km/s. Grease coupling was used in all the tests and the transducer was therefore only sensitive to plate motion in the z direction. In all the experiments the sampling frequency was 8 MHz and a 1024-($1k$) point temporal FFT was used.

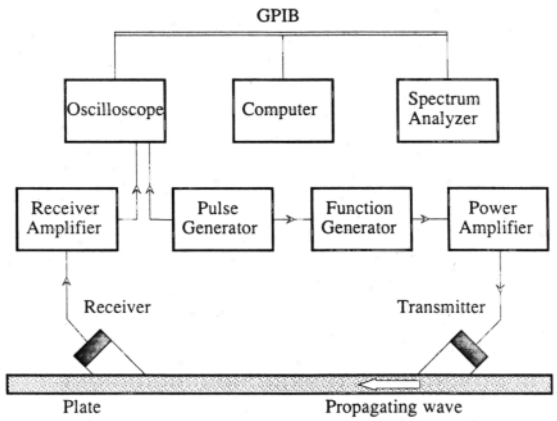

FIG. 11. Schematic representation of the experimental setup.

B. Experimental results

Figure 12(a) shows the response of a 0.5-mm-thick steel plate at 200 mm from the transmitter, where the incident angle was 28°, which was appropriate to excite and receive s_0. The frequency of the excitation tone burst was 1.2 MHz and the spatial sampling interval was 1 mm. The incident angle required for the efficient excitation and reception of a_0 at this frequency–thickness product is about 80°, so by the coincidence principle it was only very weakly excited and

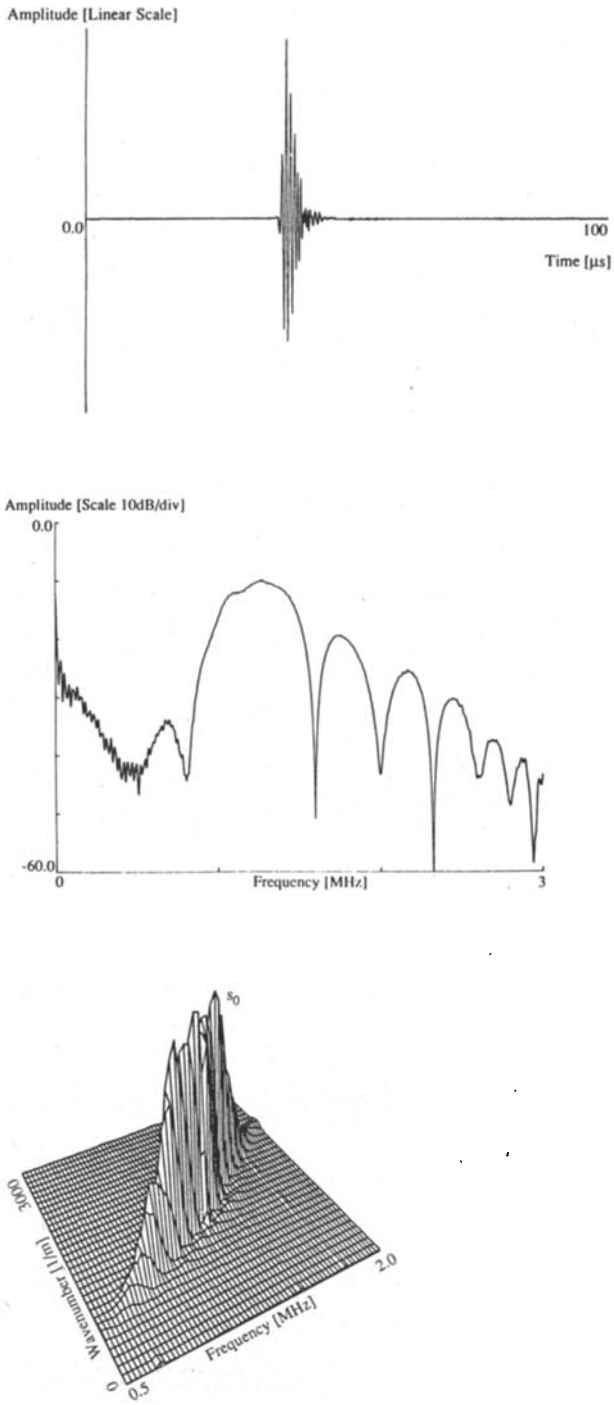

FIG. 12. (a) Normalized time history of the measured response at $x = 200$ mm in a 0.5-mm-thick plate when the excitation was appropriate for s_0. (b) Amplitude spectrum of the time history shown in (a). (c) Normalized 3-D plot of the 2-D FFT results for the case of (a).

received. This is essential, as a_0 has a low wavelength which would result in spatial aliasing for the above spatial sampling interval. Figure 12(b) shows the amplitude spectrum of the response 200 mm from the transmitter. The sidelobes in the spectrum are due to the excitation signal applied to the exciting transducer which was a simple 5-cycle tone burst, rather than a tone burst modified by a window function, such as the Hanning window employed in the numerical studies. However, the amplitudes of the sidelobes are significant only up to a frequency of around 3 MHz, so the excitation signal did not have significant energy above 1.63 MHz mm (the cutoff frequency of a_1). Therefore, since a_0 is only very weakly excited and received, s_0 should be the only mode observed and its group velocity measured using the time of flight between two points was found to be 5.35 km/s. Figure 12(c) shows the normalized three-dimensional view of the amplitude–wave-number–frequency information, which was obtained by carrying out a two-dimensional Fourier transformation of the time histories from 64 equally spaced positions between $x = 175$ mm and $x = 238$ mm. The maximum amplitude of the response of the plate is between 0.8 and 1.8 MHz. At each discrete frequency in Fig. 12(c) the wave number at which the amplitude is a maximum corresponds to the s_0 mode and, as in Fig. 4(c) no other peak is evident confirming that only the s_0 mode is observed. The dips in the amplitude of the experimental results seen in Fig. 12(c) are due to the dips in the amplitude spectrum seen in Fig. 12(b). Figure 5 shows a comparison plot, where the experimental results are denoted by triangles and were obtained by taking the wave number of the maximum amplitude at discrete frequencies in Fig. 12(c). The agreement between the theoretical, numerical, and experimental results is seen to be excellent, the maximum difference between the measured results and the theoretical predictions being less than 1%.

The amplitude of the excitation signal, the spatial pressure distribution of the transducer, and the modal properties of s_0, which are functions of frequency, all contribute to the determination of the proportion of energy available to excite the mode at a particular frequency. The mode shape and phase velocity of s_0 are almost constant in the frequency–thickness range of excitation, so the amplitude of the mode is effectively only a function of the frequency content of the excitation signal as can be deduced from Fig. 12(c).

The normalized response of a 2-mm-thick steel plate 200 mm from the transmitter, is shown in Fig. 13(a), when the input signal was intended to excite only s_0. The frequency of the excitation tone burst was 1 MHz and the spatial sampling interval used in these tests was 0.75 mm. The time history indicates that there is gross dispersion of s_0 around 2 MHz mm. Because of dispersion, the duration of the response signal is long and it is difficult to determine anything but a maximum group velocity. It is also difficult to determine whether more than one propagating mode is present from the time history plot. Figure 13(b) shows the normalized 3-D view of the amplitude wave-number–frequency information, which was obtained by carrying out a two-dimensional Fourier transformation of the time histories of 64 equally spaced positions between $x = 175$ and 222.25 mm. Two modes, s_0 and a_1, are present in Fig. 13(b). Here, s_0 is

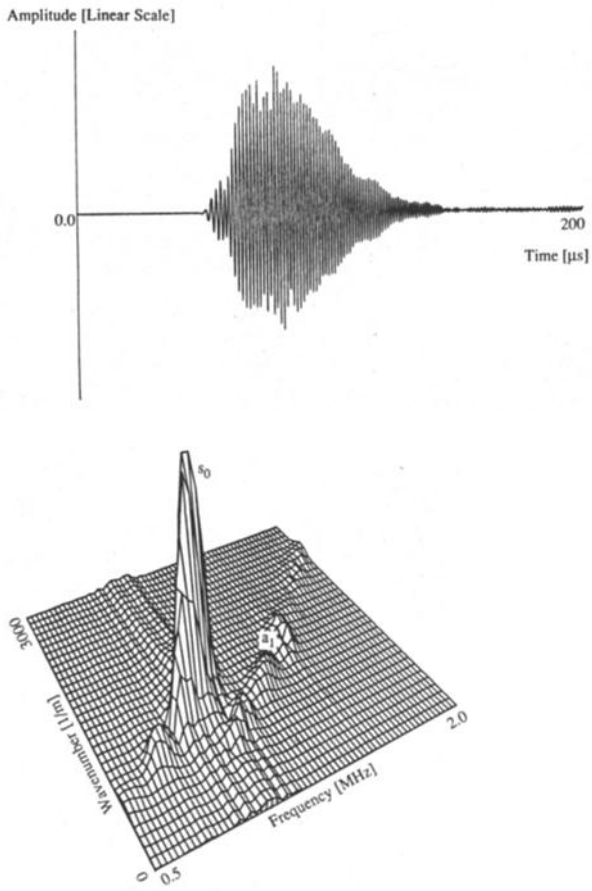

FIG. 13. (a) Normalized time history of the measured response at $x = 200$ mm in a 2-mm-thick plate when the excitation was appropriate for s_0. (b) Normalized 3-D plot of the 2-D FFT results for the case of (a).

the dominant mode and has its maximum amplitude at a frequency of 1 MHz, the center frequency of the excitation. The response reduces rapidly away from this frequency, and side lobes similar to those of Fig. 12(b) are seen. The s_0 mode is seen over a much narrower frequency range in Fig. 13(b) than in Fig. 12(c) because the frequency–thickness value is higher and the phase velocity of s_0 (and hence the coincidence angle) varies rapidly with frequency–thickness value in this range. Therefore, the excitation signal is only appropriate over a narrow range of frequencies where the wave numbers of the incident beam and the Lamb waves being excited are matched. The a_1 mode observed at higher frequencies has been excited mainly by the sidelobes of the excitation signal. In order to calculate the true amplitudes of the two modes present, the frequency content of the input signal, the pressure distribution of the transducer, the method of coupling and the mode shapes on the plate surface have to be considered.

Figure 14 shows wave-number dispersion curves for s_0 and a_1, together with experimental results obtained by locating the wave number(s) at particular frequencies at which the amplitude shown in Fig. 13(b) reaches a maximum. The agreement between the theoretical and experimental results is seen to be excellent, the maximum difference between the measured results and the theoretical predictions being less than 1%.

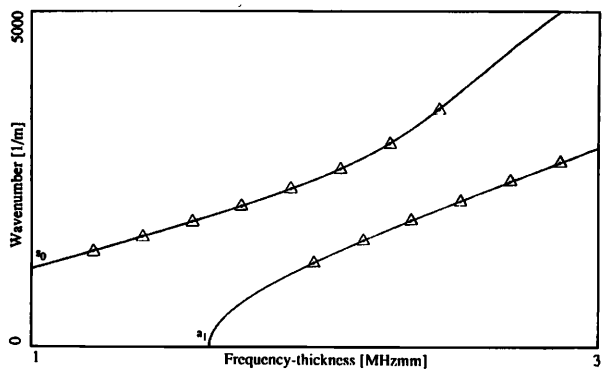

FIG. 14. A comparison of the experimental results (△) obtained from Fig. 13(b) with the theoretically computed dispersion curves (———) for s_0 and a_1.

Figure 15(a) shows the time history of the response of a 3-mm-thick steel plate 200 mm from the transmitter, when the input signal was intended to excite only a_1, the frequency of the excitation tone burst being 1 MHz. Dispersion is present, but a discrete wave packet with large amplitude is present and its group velocity indicates that it is a_1. Figure 15(b) shows the normalized 3-D view of the amplitude–wavenumber–frequency information, which was obtained by carrying out a two-dimensional Fourier transformation of the time histories of 64 equally spaced positions between $x = 175$ mm and $x = 222.25$ mm.

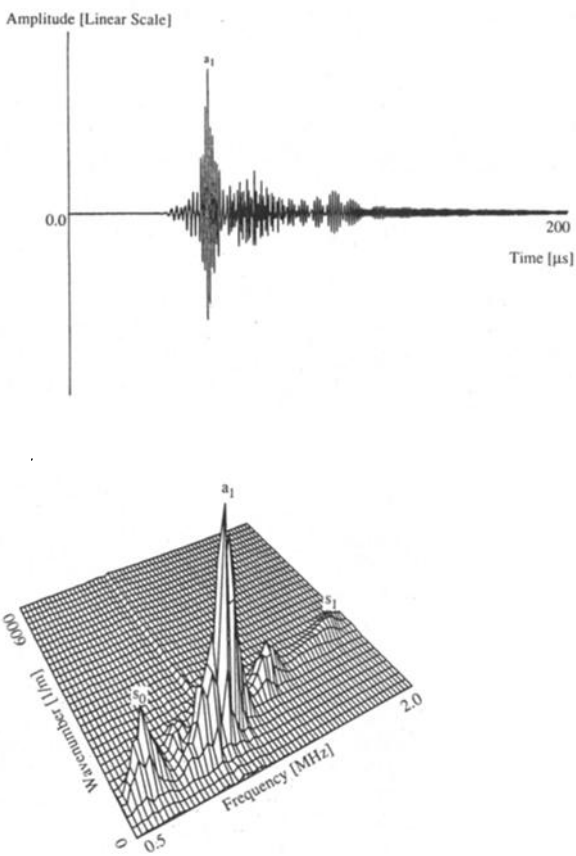

FIG. 15. (a) Normalized time history of the measured response at $x = 200$ mm in a 3-mm-thick plate when the excitation was appropriate for a_1. (b) Normalized 3-D plot of the 2-D FFT results for the case of (a).

Three modes, s_0, s_1, and a_1 are present. The different modes are observed in the frequency–thickness regions where their wave numbers and mode shapes are appropriate for their excitation and reception; a_1 dominates the response of the plate, its maximum amplitude being measured at 1 MHz, the center frequency of the excitation. Here, s_0 is seen only at frequencies below 1 MHz while s_1 is seen at higher frequencies and has being excited by the sidelobes of the excitation signal.

The experimental results show that it is very difficult to obtain a pure mode using circular variable angle transducers. The plate is excited over a range of frequencies and wave numbers, the frequency range being mainly dependent on the number of cycles in the excitation tone burst and whether a smoothing window is applied. The wave-number range is mainly dependent on the angle required and on the size of the transducers.

The effective frequency range of the excitation may be reduced by using tone bursts modulated by an appropriate window function to reduce the amplitude of the high- and low-frequency components. Experimentally, this can be achieved by using an arbitrary function generator to produce the excitation tone burst.

V. CONCLUSIONS

The 2-D FFT method has been used to measure the amplitudes and velocities of propagating Lamb waves over a range of frequencies and phase velocities in a single test. It has been shown that this technique may be used when there is multimode propagation and/or dispersion. The experimental and numerical results are in excellent agreement with theoretical predictions, the maximum difference in wave number being 1%. Although the results presented here have been for Lamb waves, the technique is equally applicable to the measurement of other propagating waves, for example, a mixture of longitudinal and shear waves.

The 2-D FFT method can be used with any Lamb wave propagation distance, subject to signal-to-noise ratio considerations. Multielement array transducers are now available, which will greatly simplify the experimental implementation of the method. The computational requirements of the 2-D FFT are fairly modest and it is anticipated that the method could readily be implemented on a microcomputer interfaced to a data capture system. This makes it attractive for NDT applications.

A method has been developed to excite a single Lamb mode in a finite element model. This will facilitate the modeling of the interaction of individual modes with defects, which will be valuable in the evaluation of Lamb waves in NDT applications.

Avioli, M. J. (1988). "Lamb wave inspection for large cracks in centrifugally cast stainless steel," EPRI report RP2405-23, Georgetown University.
Ball, D. F., and Shewring, D. (1976). "Lamb waves for inspection of commercially rolled hot strip material", Non-destructive Testing 9, 13–15.
Blake, R. J. (1988). "Numerical models of Rayleigh wave scattering from

surface features," Ph.D. thesis, Dept. of Electronic and Electrical Engineering, University of London (University College).
Bond, L. J., Punjani, M., and Saffari, N. (**1984**). "Review of some recent advances in quantitative ultrasonic NDT," IEEE Proc. **131**, Pt. A, No. 4, 265–274.
Brekhovskikh, L. M. (**1960**), *Waves in Layered Media* (Academic, New York).
Chimenti, D. E., and Nayfeh, A. H. (**1985**). "Leaky Lamb waves in fibrous composite laminates," J. Appl. Phys. **58**, 4531–4538.
Hitchings, D. (**1987**). "FE77 user manual," Imperial College internal report.
Jitsumori, A., Inoue, S., Maekawa, T., and Inari, T. (**1986**). "Generation of Lamb waves using linear array probe and its application to flaw detection," Jpn. J. Appl. Phys. Suppl. Proc. 6th Symposium Ultrasonic Electronics, Tokyo **25**, 200–202.
Mal, A. K., Yin, C.-C., and Bar-Cohen, Y. (**1988**). "The influence of the material dissipation and imperfect bonding on acoustic wave reflection from layered solids," Rev. Prog. Quant. NDE **7B**, 927–934.
Newland, D. E. (**1984**). *Random Vibrations and Spectral Analysis* (Longman, New York).
Pialucha, T., Guyott, C. C. H., and Cawley, P. (**1989**). "An amplitude spectrum method for the measurement of phase velocity," Ultrasonics **27**, 270–279.
Randall, R. B. (**1987**). *Frequency Analysis* (Bruel and Kjaer, Naerum, Denmark).
Rokhlin, S, I., and Bendec, F. (**1983**). "Coupling of Lamb waves with the aperture between two elastic plates;" J. Acoust. Soc. Am. **73**, 55–60.
Rose, J. L., Fuller, M. C., Nestleroth, J. B., and Jeong, V. H. (**1983**). "An ultrasonic global inspection technique for an offshore *K*-Joint," Soc. Petrol. Eng. J. **23**, 358–364.
Sachse, W., and Pao, Y-H. (**1978**). "On determination of phase and group velocities of dispersive waves in solids," J. Appl. Phys. **49**, 4320–4327.
Temple, J. A. G. (**1988**). "Modelling the propagation and scattering of elastic waves in inhomogeneous anisotropic media," J. Phys. D: Appl. Phys. **21**, 857–874.
Torvik, J. P. (**1967**). "Reflection of wave trains in semi-infinite plates," J. Acoust. Soc. Am. **41**, 346–353.
Viktorov. I. A. (**1970**). *Rayleigh and Lamb Waves* (Plenum, New York).
Worlton, D. C. (**1957**). "Ultrasonic testing with Lamb waves," Non-destructive Testing **15**, 218–222.
Zhang, S. Y., Zhang, S. Y., and Ying, C. F. (**1985**). "Study of the Lamb wave by the photoelastic visualization technique," in Proc. 11th World Conference on NDT, Las Vegas, pp. 1003–1007.